Kam W. Wong
Department of Civil Engineering
University of Illinois at Urbana-Champaign
Urbana, IL 61820
Alan P. Vonderohe
Department of Civil and Environmental Engineering
University of Wisconsin at Madison
Madison, WI 53706

Planar Displacement by Motion Parallax

Analytical and close-range photogrammetric techniques were used to measure displacements of sandy soils around tunnel models.

Abstract: *Analytical and close-range photogrammetric techniques were used to measure displacements of sandy soils around tunnel models. The method was based on the motion-parallax phenomenon. From the same camera position, "before" and "after" displacement photography was taken of a vertical cross-section of the tunnel model through a 9.5-mm thick glass plate. A Kodak, bellows-type, press camera with a 20 cm by 25 cm format and a 305-mm focal length Ektar lens was used for photography. Stereoscopic coordinate measurements were made on a Wild STK-1 stereocomparator. The analytical solution provided correction for instability of the camera's interior and exterior orientation between photography, and for refraction and non-planarity of the glass plate. An accuracy of ±0.08 mm and ±0.06 mm was achieved for measuring the X- and Y- components of particle displacements, respectively.*

Introduction

The method of motion parallax has long been recognized as an accurate and convenient method of measuring object movement in a plane parallel to the image plane. The basic principle is illustrated in Figure 1. A camera is positioned at point O, and an initial photograph is taken with the object located at position 1. Then, a second photograph is taken after the object has moved to position 2. Assuming that the image plane of the camera is perfectly parallel to the vertical plane containing the object's movement vector and that the camera remains perfectly stable during the entire time interval between the two exposures, the magnitude of motion in the horizontal direction, dX, can be easily computed from the following relationship:

$$dX = \frac{Z}{f} dx \qquad (1)$$

where Z is the perpendicular distance of the camera from the plane of the object's motion, f is the focal length of the camera, and dx is the displacement of the object's image in the image plane. dx is called the motion parallax and can be accurately measured using a stereocomparator or a parallax bar with a mirror stereoscope. The accuracy of the computed movement, dX, depends on the validity of the two basic assumptions, on the precision of parallax measurement, and on the scale of the photography.

Many applications of the motion parallax principle can be found in the recent literature. Hallert (1954) used the method to measure deformations on the wing of a model airplane under loading conditions and achieved a precision of ±0.03 mm. Turpin (1958) applied the method to measure deflection of pavement under heavy trucks. Finsterwald (1954), Jury (1957), and Konecny (1964) all reported on the use of motion parallax for measuring the velocity of ice movement on glaciers. Wickens and Barton (1971) used the method to measure rock deformations along a steep slope in laboratory models and claimed an

Photogrammetric Engineering and Remote Sensing,
Vol. 47, No. 6, June 1981, pp. 769-777.

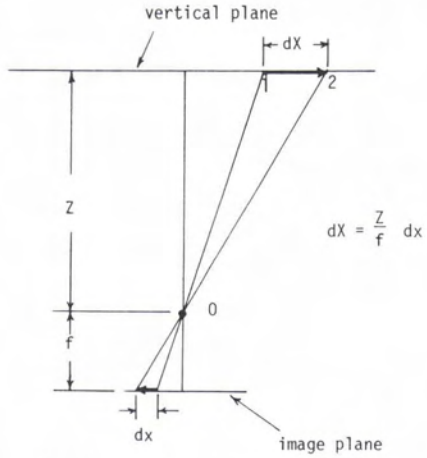

FIG. 1. Motion parallax principle.

accuracy of ±0.15 mm. Dauphin and Torlegard (1977) and Rodulescu (1978) applied the method to measure deformation in mines.

The usefulness of the motion parallax method in measuring soil displacements in laboratory models was demonstrated by Butterfield *et al.* (1970), Butterfield and Andrawes (1971), and Andrawes and Butterfield (1973). Conventionally, displacements in soil models are measured by spring-loaded strain gauges mounted on the surface of the model, and by electromagnetic strain gauges buried in the soil. Although the gauges yield displacement information at points located both on and within the model, the number of displacement points is limited by the number of gauges that can be practically installed. Moreover, the gauges themselves may influence the displacement behavior of the soil. Butterfield and Andrawes photographed the cross-section of a soil model through a glass window both before and after the occurrence of displacements. The "before" and "after" photographs were then placed in the projectors of a stereoplotter to produce a three-dimensional model of the originally flat cross-section. The relief in the model represented the amount of soil replacement in various parts of the cross-section. A procedure was developed to plot contour lines for the vertical or horizontal displacements over the entire cross-sectional area. The method did not require special targets to be buried in the soil. But the photographs had to have sufficient resolution to provide a textured surface of the soil for the purpose of stereoscopic measurement. This method had the major advantage that displacements throughout the entire cross-sectional area could be easily measured.

In the Department of Civil Engineering at the University of Illinois, the motion parallax method was recently used to supplement gauge measurements in a tunnel research project (Cording *et al.*, 1976; Vonderohe, 1980). A model was set up in the laboratory to study the effects of soil conditions and tunnel geometry on the displacement of sandy soils surrounding a tunnel. The cross-sectional area of the model to be photographed measured 1.4 m by 0.9 m, and a large-format (20 cm by 25 cm) camera was needed to obtain adequate resolution of the sand particles. In order to provide greater convenience and higher accuracy in both data reduction and analysis, a fully analytical solution was employed. Stereoscopic coordinate measurements were made on a Wild STK-1 stereocomparator. The analytical solution provided correction for instability of the camera's interior and exterior orientation between photography, and for refraction and non-planarity of the glass plate. Graphical illustrations such as displacement contours, diagrams of displacement vectors, and displacement profiles could be generated directly from the computer.

The Tunnel Model

As shown in Figure 2, the tunnel model was housed in a steel-framed box which had a 9.5-mm thick glass plate at one of the longitudinal sides. A 152-mm diameter steel pipe represented the tunnel lining and a close-fitting, larger diameter brass pipe represented the construction shield. The soil surrounding the tunnel consisted of well-graded sand with grain sizes ranging from 0.2 mm to 0.8 mm. The density of the sand was controlled by varying the height of fall during its placement and by the degree of compaction.

During a test, the larger diameter construction shield was winched away from the glass plate at incremental distances. As the shield was winched away, the sand particles surrounding the model moved in to fill the void. The objective of the study was to measure the directions and magnitudes of the particle movements at various distances from the tunnel.

To serve as photogrammetric control points, eleven targets were attached to the outside face of the glass plate. The distances between these targets were measured with a calibrated meter bar to ±0.1 mm. The X and Y coordinates of these targets were then computed by the method of least-squares. The solution had 21 degrees of freedom, and the maximum standard error in the computed X and Y coordinates amounted to ±0.09 mm.

The index of refraction, N, of the glass plate was determined to be 1.428 ± 0.015.

Data Acquisition

When the steel-framed box was filled with sand, the glass plate itself was distorted from a truly planar surface by load exerted by the sand. Prior to photography during each test, the curvature of the glass plate was measured by a rectangular array of

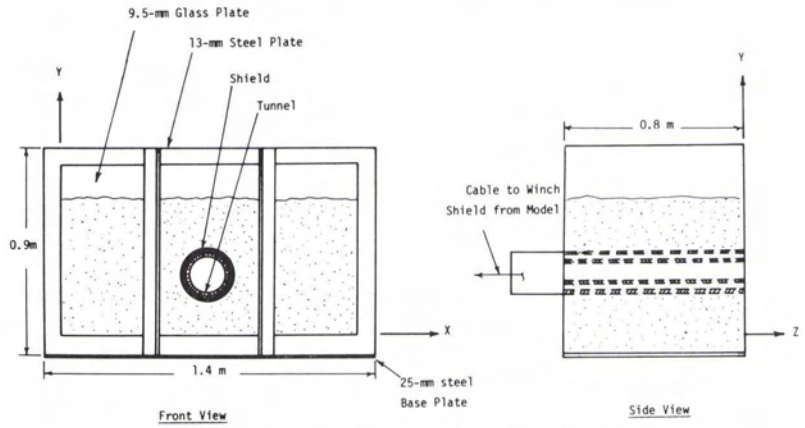

FIG. 2. Schematic drawing of the tunnel model.

25 strain gauges. Figure 3 illustrates the typical distortion pattern. The distortion vectors were perpendicular to the planar position of the glass plate and towards the camera.

A permanent camera stand was bolted to the floor at a distance of approximately 1.8 m in front of the glass plate. There was no large change in the camera position from test to test. A Kodak bellows-type press camera with a 20 cm by 25 cm format and a 305-mm focal length Ektar lens was used for photography. It was the only camera which had the required resolution and which could be conveniently made available for this study. The bellows were braced during the test in order to minimize the changes in the interior orientation of the camera. Kodak Plus X Pan film with an ASA rating of 200 was used. At the stated object distance of 1.8 m, the cross-sectional view of the model virtually filled the entire photograph as shown in Figure 4, which is a reduced copy of an actual photograph used for measuring particle movement.

An initial "no-movement" photograph was taken with the end of the construction shield being in contact with the inside face of the glass plate. The shield was then winched away from the plate in increments of six inches. After each incremental move, a photograph was taken. For the sake of clarity, throughout the remainder of this paper, the initial photograph will be referred to as "photo 1" and any subsequent photograph taken after the tunnel shield had been moved will be referred to as "photo 2."

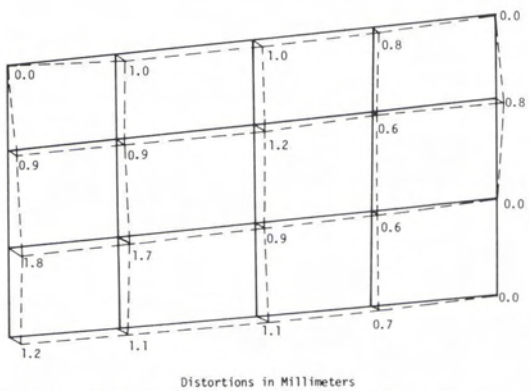

FIG. 3. Typical distortion of glass plate under load.

During each test, spring loaded strain gauges, as are visible in Figure 4, were mounted on the top surface of the sandy soil, and electromagnetic strain gauges were buried along a vertical line just above the center line of the tunnel model and located at a distance of about 13 inches inward from the glass plate. These gauges were read after each incremental move of the shield. These gauge readings measured the displacements in the vertical direction only.

Stereoscopic coordinate measurements were made on a Wild STK-1 stereocomparator. Photo 1 was placed on the right stage plate of the comparator and photo 2 was placed on the left stage plate. The y-axes of the photographs were made approximately parallel with the x-axis of the comparator. This arrangement of the photographs served two purposes. First, since the largest component of particle movement was along the vertical (or y) direction, this arrangement dramatized the apparent relief in the sand surface caused by motion parallax. Second, this arrangement permitted the y-component of movement to be measured more accurately than the x-component. The coordinates of all eleven control points as well as about 350 other points well distributed over the cross-sectional area were usually measured. Plate 1 shows the relevant portion of a stereoscopic pair of photographs. The motion parallax can be viewed as a depression to the right of the circular tunnel.

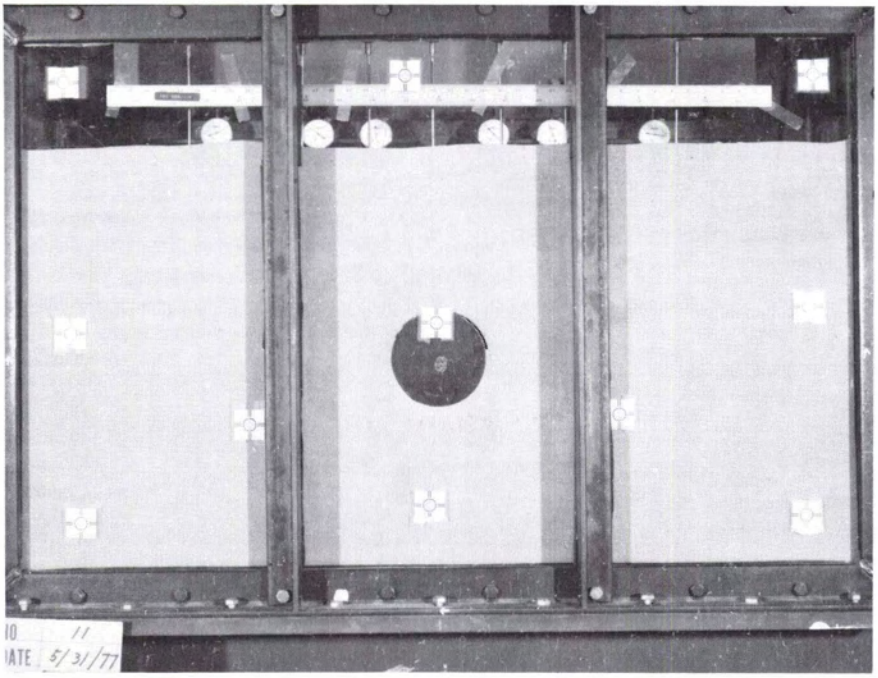

FIG. 4. Sample photograph for measuring particle movement (reduced for publication).

THE ANALYTICAL SOLUTION

Figure 5 illustrates the general steps involved in the analytical solution for the movement vectors. Initially, the comparator coordinates were transformed to a photo coordinate system. The camera did not have a set of fiducial marks to define the photo coordinate system. Moreover, the format of the photo was so large that neither the edges nor the corners of the photographs could be measured on the Wild STK-1 stereocomparator. Consequently, the x- and y-axes of the photographic coordinate system were determined only approximately for each photograph. Figure 6 illustrates the measurements used to define the photo coordinate system. A precision rule was used to measure the lengths of the four edges of a photograph (l_1, l_2, d_1, and d_2) and the perpendicular distances (p_1, g_1, p_2, and g_2) of two control points from the two closest edges of the photograph. The photo coordinates of the two control points were then defined as follows:

$$x_1 = -\tfrac{1}{4}(l_1 + l_2) + p_1 \quad (2)$$

$$y_1 = -\tfrac{1}{4}(d_1 + d_1) + g_1 \quad (3)$$

$$x_2 = \tfrac{1}{4}(l_1 + l_2) - p_2 \quad (4)$$

$$y_2 = \tfrac{1}{4}(d_1 + d_2) - g_2 \quad (5)$$

which effectively defined the photo coordinate system.

The exterior orientation of photo 2 with respect to photo 1 was then determined by a computer subroutine, which performed a least-squares solution for a three-dimensional coordinate transformation. It made use of the following basic projective transformation equations:

$$\begin{bmatrix} x_j \\ y_j \\ z_j \end{bmatrix} = \lambda_j \begin{bmatrix} m_{11} & m_{12} & m_{13} \\ m_{21} & m_{22} & m_{23} \\ m_{31} & m_{32} & m_{33} \end{bmatrix} \begin{bmatrix} X_j - X^c \\ Y_j - Y^c \\ Z_j - Z^c \end{bmatrix} \quad (6)$$

where x_j, y_j, and z_j are the photo coordinates of an image point; X_j, Y_j, and Z_j are the object space coordinates of the corresponding point in the object space; λ_j is a scale factor: X^c, Y^c, and Z^c are the object space coordinates of the exposure center of the photograph; and the m_{ij}'s are functions of the three rotation parameters ω, ϕ, and κ.

In the solution for the exterior orientation of photo 2 with respect to photo 1, the photo coordinates of the eleven control points measured in photo 1 were used as controls. The subroutine solved for the three rotation parameters $\bar{\omega}_2$ $\bar{\phi}_2$, and $\bar{\kappa}_2$ and three translation parameters $\bar{X}_2^c$, $\bar{X}_2^c$, and Z_2^c of photo 2.

Using the same subroutine, the orientation of photo 1 with respect to the control points in the object space was next determined. The solution solved for three rotation parameters ω_1, ϕ_1, and κ_1, and three translation parameters X_1^c, Y_1^c, and Z_1^c of photo 1. Eleven control points were used in the solution.

The parameters ω_1, ϕ_1, κ_1, X_1^c, Y_1^c, and Z_1^c were then used to compute the object space coordinates of the image points in photo 1. The three-dimensional projective transformation equations

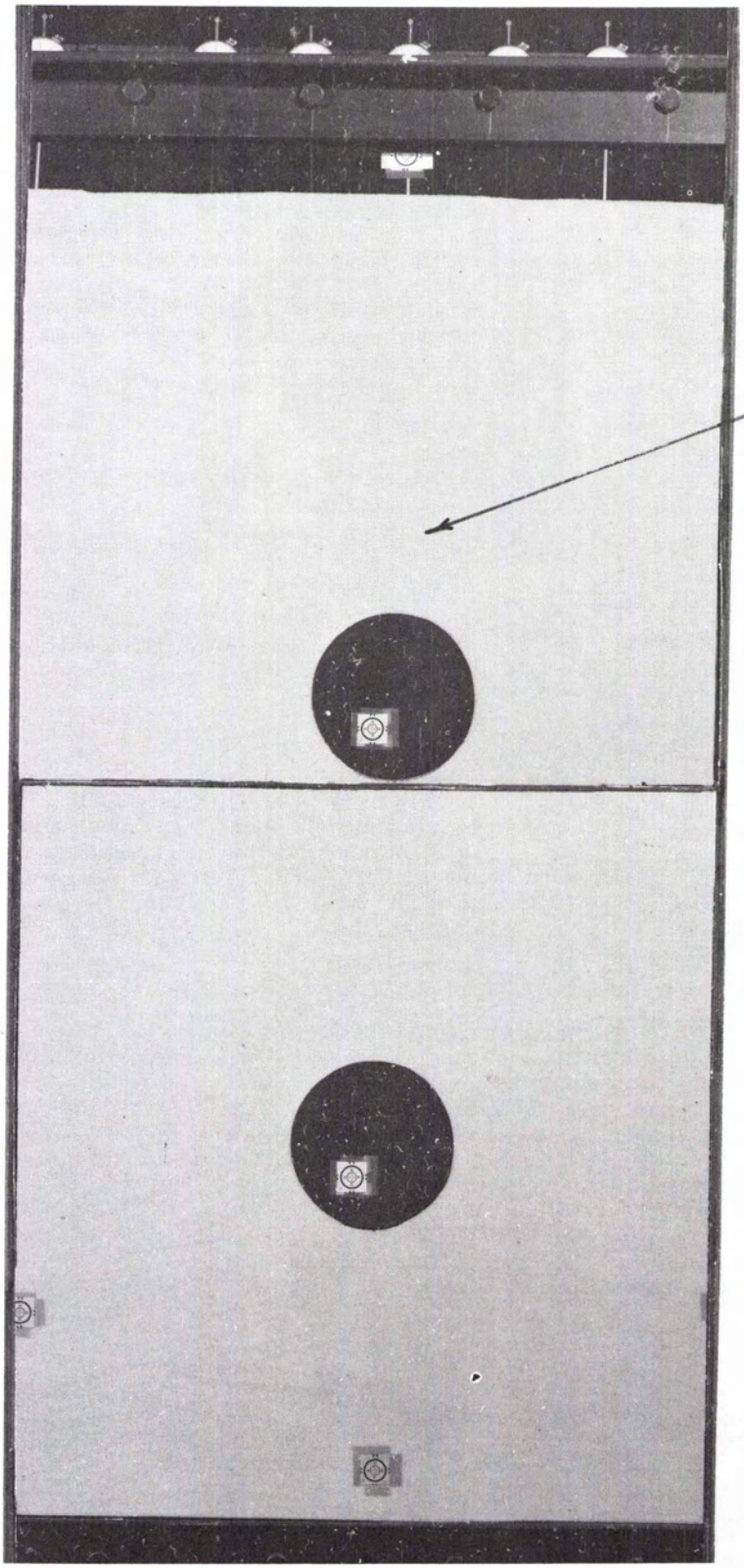

PLATE 1. Relevant portion of a stereoscopic pair of photographs.

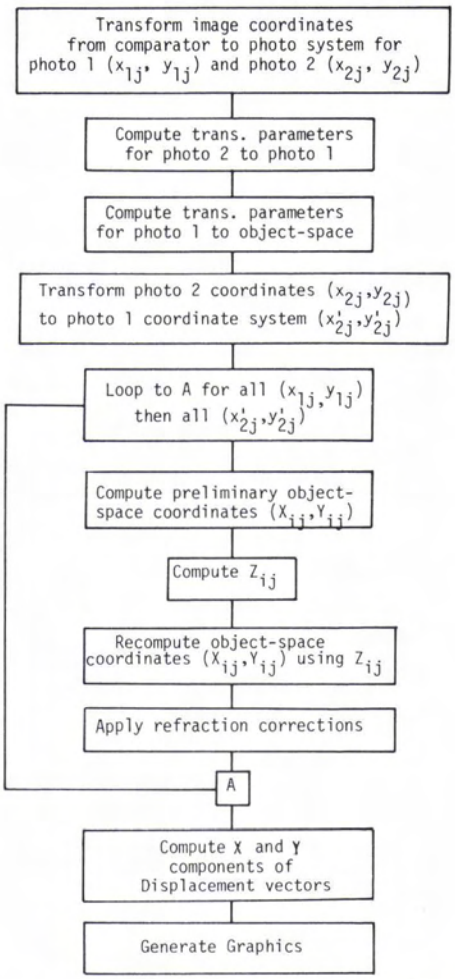

FIG. 5. General steps in the analytical solution.

were used in a two-step solution. Let x_{1j} and y_{1j} represent the image coordinates of point j in photo 1; and X_{1j}, Y_{1j}, and Z_{1j} represent the corresponding object space coordinates of the same point. Because of the deflection of the glass plate, the cross-sectional surface of the model was not a true planar surface and Z-coordinates were not all equal to zero. In the first step, approximate values of the X_{1j} and Y_{1j} coordinates were computed by assuming that $Z_{1j} = 0$. These approximate coordinates were then used to compute the actual Z-deflection of the glass plate. This was accomplished by using an inverse-weighted distance function and the four nearest data points obtained from strain gauge measurements. The Z_{1j} coordinate was then used to recompute the X_{1j} and Y_{1j} coordinates of point j.

The object space coordinates X_{2j}, Y_{2j}, and Z_{2j} of the same point j after a certain movement of the construction shield were then computed from photo 2. Let x_{2j} and y_{2j} represent the photo coordinates of point j measured from photo 2. These coordinates were first transformed to the photo 1 system using the orientation parameters $\bar{\omega}_2$, $\bar{\phi}_2$ $\bar{\kappa}_2$, $\bar{X}_2^c$, and $\bar{Y}_2^c$. This step corrected for the effects of any movement of the camera between exposures. Let x'_{2j} and y'_{2j} represent the transformed photo coordinates of point j. Then, the corresponding object space coordinates X_{2j}, Y_{2j}, and Z_{2j} were computed using the orientation parameters ω_1, ϕ_1, κ_1, and X_1^c, Y_1^c, and Z_1^c and the same procedure as that described in the above paragraph. The computed coordinates X_{1j}, Y_{1j}, X_{2j}, and Y_{2j} were then corrected for refraction. The refraction correction, dX and dY, for the coordinates X_{1j} and Y_{1j} was computed from the following expressions:

$$\psi = \tan^{-1}\left((X_{1j} - X_1^c) / (Y_{1j} - Y_1^c)\right) \quad (7)$$

$$\alpha = \tan^{-1}\left(((X_1^c - X_{1j})^2 + (Y_1^c - Y_{1j})^2)^{1/2} / (Z_1^c - Z_{1j})\right) \quad (8)$$

$$\beta = \sin^{-1}(\sin \alpha / N) \quad (9)$$

$$d = T(\tan \alpha - \tan \beta) \quad (10)$$

$$dX = d \cdot \mathrm{Sin}\ \psi \quad (11)$$

$$dY = d \cdot \mathrm{Cos}\ \psi \quad (12)$$

where N is the index of refraction and T is the thickness of the glass plate. The refraction corrections were then applied by the following expressions:

$$X'_{1j} = X_{1j} + dX$$
$$Y'_{1j} = Y_{1j} + dY$$

Let X'_{2j} and Y'_{2j} be the corresponding corrected coordinates from photo 2. The movement components of point j in the X and Y directions during the time interval between the two exposures were then computed as the changes in the corrected coordinates, i.e.,

$$\Delta X = X'_{2j} - X'_{1j} \quad (13)$$
$$\Delta Y = Y'_{2j} - Y'_{1j} \quad (14)$$

Since the displacement vectors were in numerical form, many different graphical illustrations could be directly generated from the computer. Figure 7 is an example of a plot of the movement vectors at points around the tunnel model. Figure 8 is a profile plot of vertical displacement near the

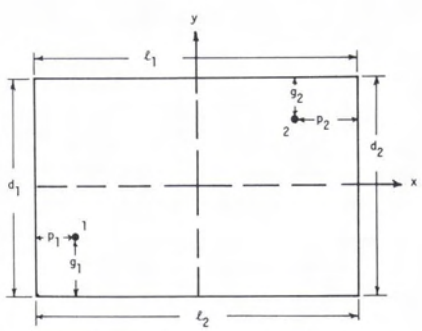

FIG. 6. Definition of photo coordinate system.

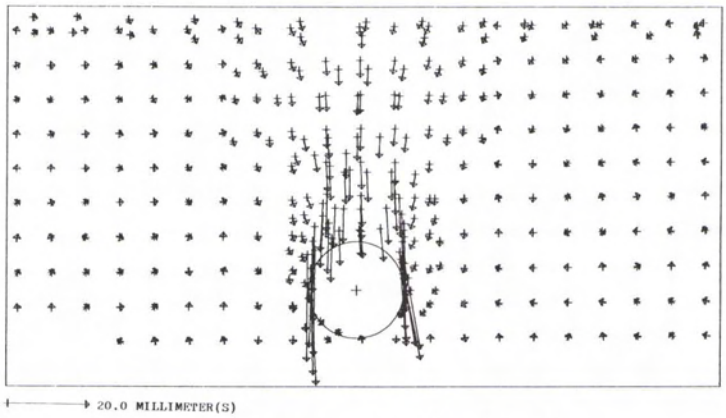

FIG. 7. Movement vectors of sand particles.

soil's surface. The plot shows the vertical displacements along a fixed profile after the construction shield (i.e., the outside pipe) had been pulled to a distance of 6, 18, and 30 inches behind the glass plate. Thus, the data for the plot were derived from parallax measurements made on three different stereoscopic pairs of photos. The three sets of measurements indicate incremental displacements for the different positions of the construction shield. Figure 9 is a profile plot of the corresponding horizontal displacements. Contour plots can also be generated for the X and Y components of movement separately, and for strain distributions throughout the cross-sectional area of the model.

ACCURACY ANALYSIS

In order to test the overall accuracy of the method, two photographs were taken of the tunnel model in its undisturbed position. These two photographs were then measured and analyzed as a pair of "before" and "after" photographs. Figure 10 is a plot of the computed displacement vectors which, in fact, are measurement errors. If the system of measurement was totally free of error, there would have been zero displacement at all points

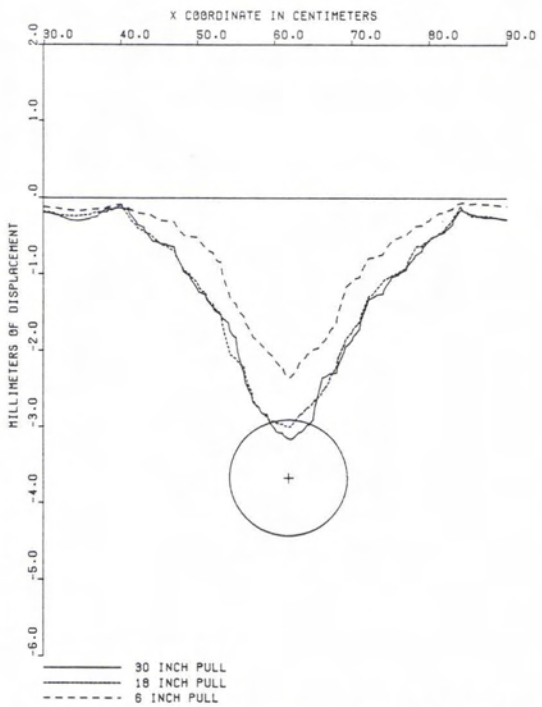

FIG. 8. Y-displacements near surface of the model.

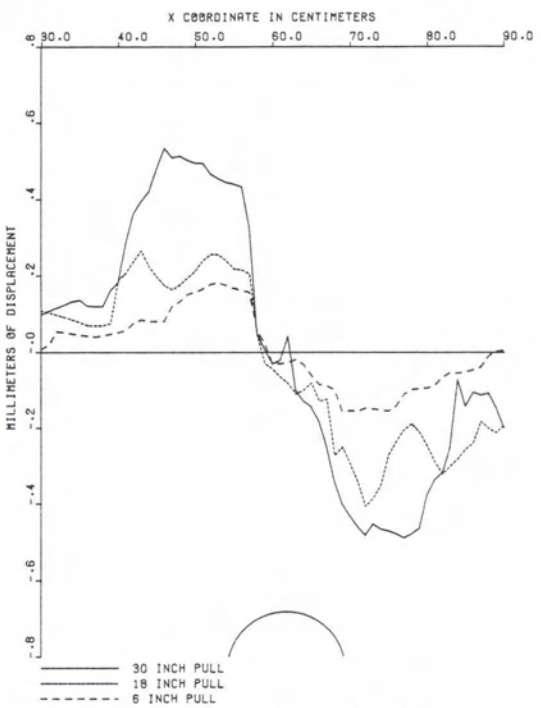

FIG. 9. X-displacements near surface of the model.

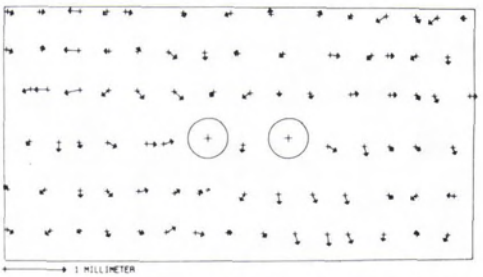

FIG. 10. Error vectors in a displacement-free test.

within the model area. The average and standard deviation of the X and Y components of the 84 error vectors in Figure 10 were as follows:

	Displacement error	
	X-component	Y-component
Average	+0.01 mm	−0.04 mm
Standard deviation	±0.08 mm	±0.04 mm

The average errors of +0.01 mm and −0.04 mm. were most likely caused by small residual errors in the relative orientation of photo 2 with respect to photo 1. For example, an error of 5 seconds of arc in the ω rotation would result in an average error of 0.05 mm in the Y component of displacements. The random components of the error vectors in Figure 10 represent the combined effects of all other sources of errors, including errors in the parallax measurements, lens distortion, film distortion, and errors in the interior orientation parameters of the camera.

For each pair of "before" and "after" photographs, there were many points which were located near the outside edges of the tunnel model where no displacement was expected. Thus, any displacements computed at such points could be considered as measurement error. Listed in Table 1 are the means and standard deviations of the error vectors computed at such points for four different experiments. The overall average standard deviations for the four tests, including 129 check points, were ±0.08 mm and ±0.06 mm for the X- and Y-components respectively. These magnitudes are in excellent agreement with those obtained from the displacement-free test discussed in the above paragraph.

It was concluded that the instrumentation and procedure could yield an accuracy of ±0.08 mm and ±0.06 mm in measuring the X and Y components of particle movement respectively. The systematic errors caused by any residual errors in the relative orientation of photo 2 to photo 1 could be determined from the check points, and corrections could be applied to all the displacement vectors.

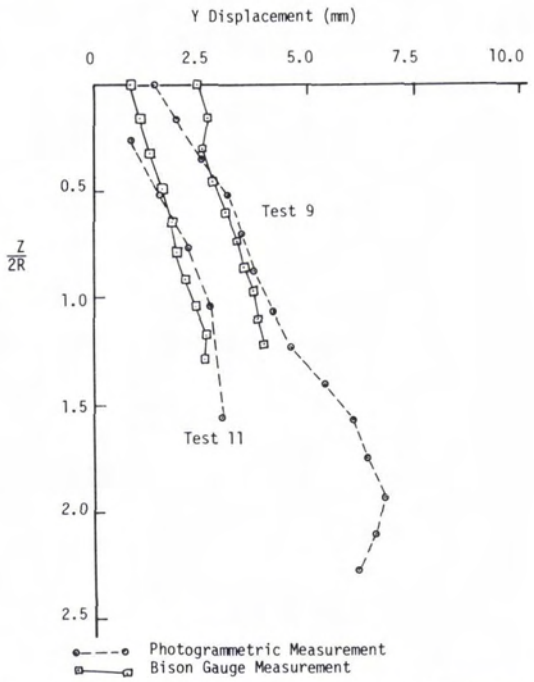

FIG. 11. Comparison of Bison gauge and photogrammetric measurements.

Figure 11 shows a comparison of the photogrammetric and gauge measurements of displacements above the tunnel crown for two tests. In the figure, vertical displacement is plotted against the parameter $Z/2R$, where Z is the depth of the data point beneath the surface and R is the radius of the tunnel model. There was good agreement between the two sets of measurements in both tests. However, a rigorous analysis of the accuracy of the photogrammetric measurements could not be made from the gauge measurements. While the photogrammetric method measured the particle

TABLE 1. DISPLACEMENT ERRORS COMPUTED FROM FOUR EXPERIMENTS

Experiment	No. of Check Points	d_X^*	σ_X^{**}	d_Y^*	σ_Y^{**}
1	26	0.044	0.111	0.014	0.066
2	38	0.040	0.068	0.006	0.057
3	47	0.034	0.076	−0.028	0.062
4	18	0.007	0.063	−0.028	0.058
Mean	129	0.03	0.08	−0.009	0.06

* d_X, d_Y means of X and Y components of error vectors.
** σ_X, σ_Y Std. deviation of X and Y components of error vectors.

movement against the glass plate, the gauges were buried along a vertical line situated about 13 inches behind the glass and actually measured particle movements within the sand model. Because of physical constraints, gauges could not be placed directly behind the glass plate. The density of the sand located near the glass plate might also differ from the density in the interior. In addition, since the measuring surface of a gauge was a small glass disk, it could only measure the average settlement below the disk. However, primarily because of these differences in the two methods of measuring displacements, the photogrammetric method played a major role in measuring the behavior of the model under various test conditions.

Conclusions

The analytical approach provided an effective method of correcting for the effects of camera motion between exposures, refraction, and nonplanarity of the glass plate. Displacement vectors could be determined with a root-mean-square (RMS) error of ±0.08 mm and ±0.06 mm for the horizontal and vertical components, respectively, corresponding to ±0.014 mm and ±0.008 mm, respectively, at the scale of the photographs.

The experimental results showed that the accuracy of the method was largely limited by the accuracy of parallax measurements. Although the Wild STK-1 stereocomparator has a least count of ±0.001 mm, the RMS error of parallax measurements was estimated to be about ±0.005 mm. The fine texture of the sand grains presented a poor surface for stereoscopic measurements and accounted for the relatively large errors in parallax measurement.

In future applications of this method, the effects of film distortion can also be minimized by etching a grid on the inside face of the glass plate. The grid intersections then would provide a network of check points throughout the entire object field. Displacements at these check points should theoretically be zero. Thus, any systematic displacements measured at these points could be used to apply corrections to the surrounding object points.

Because of the relatively small magnitude of the displacement vectors (usually less than 10 mm), and since all the large displacements were confined to the center part of the photographs, lens distortion did not significantly affect the precision of the measurements in this experiment. Should the effects of lens distortion become significant, well-known procedures are available for the calibration and correction of lens distortions.

Acknowledgment

This study was conducted in cooperation with Professor E. J. Cording, of the Department of Civil Engineering at the University of Illinois at Urbana-Champaign, as a part of a study on tunnel design and construction which was supported by the U.S. Department of Transportation. All the soil tests on the tunnel models were conducted under the direction of Professor Cording. Mr. P. Lenzini, a graduate student in Civil Engineering, played a major role in the design of the tunnel model; and Mr. S. W. Hong, a graduate research assistant, was responsible for conducting the tests and for analysis of the gauge measurements.

References

Andrawes, K. Z., and R. Butterfield, 1973. The Measurement of Planar Displacements of Sand Grains, *Geotechnique*, Vol. 23, No. 9, pp. 571-576.

Butterfield, R., R. M. Harkness, and K. Z. Andrawes, 1970. Stereo-photogrammetric Method for Measuring Displacement Fields, *Geotechnique*, Vol. 20, No. 3, pp. 308-314.

Butterfield, R., and K. Z. Andrawes, 1971. The Visualization of Planar Displacement Fields, *Proceedings, Roscoe Memorial Symposium*, Cambridge, pp. 467-475.

Cording, E. J., W. H. Hansmire, H. H. MacPherson, P. A. Lenzini, and A. P. Vonderohe, 1976. *Displacements Around Tunnels in Soil*, Dept. of Civil Engineering, University of Illinois at Urbana-Champaign, Urbana, Illinois, Report No. DOT-TST 76T-22, prepared for U.S. Dept. of Transportation.

Dauphin, E., and K. Torlegard, 1977. Displacement and Deformation Measurements Over Longer Periods of Time, *Photogrammetria*, Vol. 33, No. 6, pp. xxx.

Finsterwald, R., 1954. Photogrammetry and Glacier Research with Special Reference to Glacier Retreat in the Eastern Alps, *Journal of Glaciology*, Vol. 2, No. 15, pp. xxx.

Hallert, B., 1954. Deformation Measurements by Photogrammetric Methods, *Photogrammetric Engineering*, Vol. 20, No. 5, pp. xxx.

Jury, H., 1957. An Application of Photogrammetry to Glaciology in Greenland, *Photogrammetric Engineering*, Vol. 23, No. 3, pp. xxx.

Konecny, G., 1964. Glacier Survey in Western Canada, *Photogrammetric Engineering*, Vol. 30, No. 1, pp. xxx.

Radulescu, D., 1978. Photogrammetric Determinations on Equivalent Models in Mining Industry Studies, *Proceedings, Inter-Congress Symposium*, International Society of Photogrammetry-Commission V, Stockholm, Sweden.

Turpin, R. D., 1958. Photogrammetric Techniques for Engineering Measurements, *Photogrammetric Engineering*, Vol. 25, No. 5, pp. xxx.

Vonderohe, A. P., 1980. *Photogrammetric Systems for the Analysis of Planar Displacements in Soil*, Ph.D. dissertation, Department of Civil Engineering, University of Illinois at Urbana-Champaign, Illinois, In preparation.

Wickens, E. H., and N. R. Barton, 1971. The Application of Photogrammetry to the Stability of Excavated Rock Slopes, *Photogrammetric Record*, Vol. 7, No. 37, pp. xxx.

(Received 28 August 1980; accepted 9 December 1980; revised 28 December 1980)